International Journal of Computer Assisted Radiology and Surgery (2018) 13:1439–1451
https://doi.org/10.1007/s11548-018-1783-x

ORIGINAL ARTICLE

Robust path planning for flexible needle insertion using Markov decision processes

Xiaoyu Tan[1] · Pengqian Yu[2] · Kah-Bin Lim[1] · Chee-Kong Chui[1]

Received: 4 December 2017 / Accepted: 3 May 2018 / Published online: 11 May 2018

Abstract

Purpose Flexible needle has the potential to accurately navigate to a treatment region in the least invasive manner. We propose a new planning method using Markov decision processes (MDPs) for flexible needle navigation that can perform robust path planning and steering under the circumstance of complex tissue–needle interactions.

Methods This method enhances the robustness of flexible needle steering from three different perspectives. First, the method considers the problem caused by soft tissue deformation. The method then resolves the common needle penetration failure caused by patterns of targets, while the last solution addresses the uncertainty issues in flexible needle motion due to complex and unpredictable tissue–needle interaction.

Results Computer simulation and phantom experimental results show that the proposed method can perform robust planning and generate a secure control policy for flexible needle steering. Compared with a traditional method using MDPs, the proposed method achieves higher accuracy and probability of success in avoiding obstacles under complicated and uncertain tissue–needle interactions. Future work will involve experiment with biological tissue in vivo.

Conclusion The proposed robust path planning method can securely steer flexible needle within soft phantom tissues and achieve high adaptability in computer simulation.

Keywords Robust planning · Needle steering · Tool–tissue interaction · Markov decision processes · Uncertainty

Introduction

Minimally invasive surgery (MIS) has significantly reduced surgical injury and enhanced postoperative recovery [1,2]. Percutaneous MIS has been performed for diagnosis and therapies [3]. These percutaneous approaches involve inserting needles through the skin and into the homological stiff tissue to reach the target region. The needles are inserted usually under ultrasound, CT or X-ray guidance [4].

Precision is one of the most important considerations in percutaneous MIS [5]. Many clinical studies show that the problems of percutaneous approaches are image limitations and misalignment [6], the complex properties in treatment areas [7], tissue deformation and uncertainty in needle–tissue interaction [8,9]. Another major issue of implementing percutaneous MIS is avoiding subsequent damage. The targets might be blocked by other tissues which may contain crucial organs and vessels [10].

To overcome the difficulties mentioned above in percutaneous approaches, we developed a new robust path planning method using MDPs that could provide secure and optimal action sequence for steering flexible bevel-tip needles. These needles could be controlled in two degrees of freedom to follow the particular curving trajectory [11,12].

In this paper, we first constructed a 2D model based on segmented medical image for the needle misplacement problem caused by tissue deformation [6,8]. Then, to penetrate the treatment area with higher probability [13–15], a

✉ Xiaoyu Tan
xiaoyu_tan@u.nus.edu

Pengqian Yu
yupengqian@u.nus.edu

Kah-Bin Lim
limkahbin@nus.edu.sg

Chee-Kong Chui
mpecck@nus.edu.sg

[1] Department of Mechanical Engineering, National University of Singapore, Singapore 117575, Singapore

[2] Department of Industrial Systems Engineering and Management, National University of Singapore, Singapore 117576, Singapore

new algorithm is developed to adjust the insertion direction toward the treatment area in the context of MDPs. This problem [16] was not discussed in other works [9,17–19].

Although the uncertainty in tissue–needle interaction is parameterized as transition probability and discussed in some works [9,20,21], the uncertainty of these parameters is highly varying and usually within an interval due to non-homogeneous nature of soft tissue [10]. Using one transition probability to represent a range of uncertainty in needle–tissue interaction is not sufficient in practical application. Hence, to enhance the robustness and prevent the worst cases under a range of transition probability in MDPs, a recent work on parameter uncertainty [22] is implemented to generate a more robust control action sequence under uncertainties.

To investigate the viability of our proposed robust path planning method, computer simulations and phantom experiments are conducted to show the improvement compared with traditional MDPs steering algorithm [9,20,21]. The results also show the feasibility in steering a flexible needle with robotic manipulator. Based on the experimental results, with a segmented medical image of the targets and obstacles, the robust path planning method can generate a more optimal and secure action sequence to control the flexible needles in a more realistic situation compared to the traditional MDPs framework [9,20,21].

Related works

The concept of needle steering and path planning was defined in research [23,24], as the motion to control the orientation and position of the needle to perform the MIS percutaneous therapies.

Inverse kinematic algorithms could be implemented in path planning and needle steering. Given the direction and location of the needle tip trajectory, the translation and direction with respect to the needle base could be achieved [25]. Another model-based algorithm proposed a non-homogeneous model to simulate the trajectory of flexible needle with image guidance [26].

To make further improvement in accuracy and robustness of needle steering, many algorithms using real-time medical imaging were introduced. A rapid re-planning algorithm was developed to steer the needle with rapidly exploring random tree (RRT) planner in 3D surgical circumstance [19]. Another similar approach used RRT to perform the needle steering under 2D ultrasound images in 3D non-static surgical environment [18]. A new algorithm was developed by performing strain measurement from fiber Bragg grating (FBG) sensors and tracking the needle position with ultrasound-based tracking algorithm [27].

However, there are limitations with these methods utilizing real-time medical imaging. Compared with off-line preoperative medical images, the real-time medical imaging does not provide accurate registration and distinct features for both treatment areas and surgical tools [28]. If ultrasound imaging is used to monitor needle insertion, the ultrasound probe may push the patient skin and shift the target location. The fluoroscope also increases X-ray exposure for both patient and physician.

Therefore, other flexible needle steering frameworks were developed to handle both preoperative and real-time medical imaging models [9,20,21]. There are algorithms that implement MDPs [29] and dynamic programming (DP) [30] in postoperative model and calculate the optimal trajectory of steerable needle insertion without invading sensitive tissue. Their methods also contribute to solving the issue of robotic control failure under the uncertainty of needle–tissue interaction [9]. However, a simplex probability prediction of uncertainty in one specific area is not sufficient since the properties for each patients are always varying in a certain range. The real uncertainty of tissue deformation which may follow a normal distribution [13–15] should also be fully considered in path planning phase to achieve more robust and accurate results.

Therefore, we propose a new robust path planning method to provide secure and optimal motion planning for needle–tissue interaction. This method follows the previous work [9,20,21] that incorporates distributionally robust counterpart [22] and multiple deformation researches in liver tissues [13–15].

Methodology

After an overview of the basic motion planning, we describe our robust path planning method and its implementation. The flow chart shown in Fig. 1 indicates the three major procedures of the robust path planning method. Each procedure addresses one core issue in flexible needle steering.

This method uses segmented CT images to generate a basic map which contains the shape of obstacles. The segmentation could be performed by physicians or using various machine learning methods [31,32]. Since this part is not covered by the robust path planning algorithm, only the CT images segmented by medical professionals are discussed in this paper.

The method is validated on a simulated robot-assisted radio-frequency ablation (RFA) surgery with real patient's CT data and a phantom RFA needle insertion experiment using a prototype surgical robot [33,34] developed by our research group.

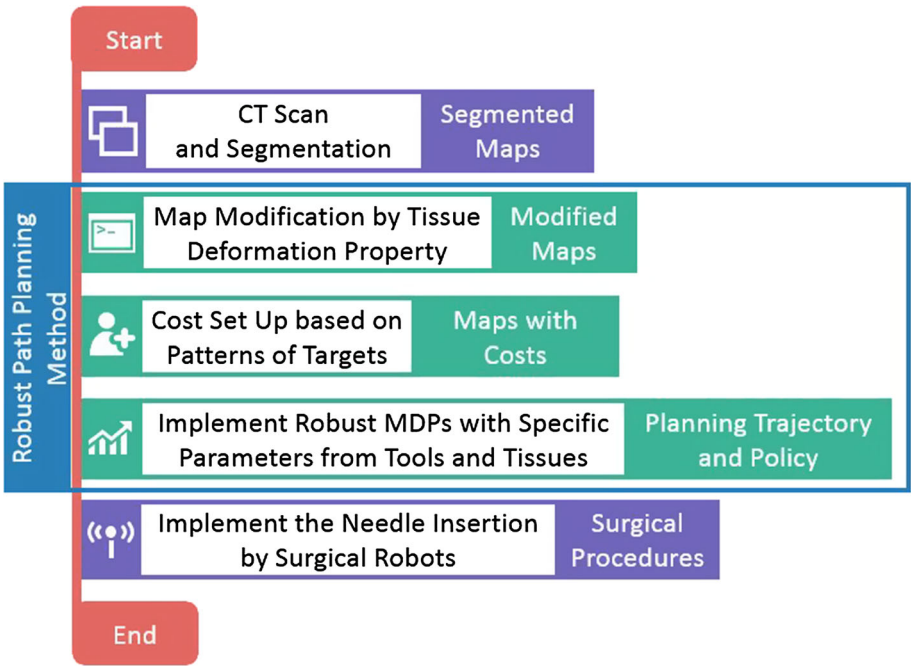

Fig. 1 The flow diagram of robust path planning method in surgical robotic needle insertion

Step one: map modification by using tissue deformation properties

In practice, thin bevel-tip needles which are widely applied in biopsy can cause minuscule tissue deformation [11], and other flexible bevel-tip needles used in medical treatment will also lead to non-negligible tissue deformation [13–15]. To maximally avoid obstacles in the treatment area, the deformation behavior should be considered in the robust path planning method.

In this procedure, we consider indentation and compression behavior [14,35] which occurred in navigating the surgical instruments inside the tissue. These two types of deformation will influence the patterns of obstacles and potentially increase the risk of damaging obstacles in needle steering.

The obstacles represented in maps could be important internal organs, vessels, bones or other sensitive tissues. Although the sensitive tissues may have higher stiffness compared with that of normal tissues, these tissues are surrounded and adhered by normal organ tissues and are also affected by stress effect due to tissue deformation. The proposed algorithm is developed to avoid these obstacles aiming for minimal chance for inserting the needle directly into the obstacles. Therefore, simulating the deformation behavior by applying normal tissue properties can maximally realize the purpose of robust path planning for tissue deformation.

We compare our method with the traditional MDPs path planning framework [9,20,21]. In this framework, the needle will insert a unit distance δ in normal tissue. This framework was developed based on assumption that the deformation behavior is negligible. However, the tissue around the needle tip will be compressed due to the stress given by the extrusion of needle tip and the curvature of whole needle. Hence, when needle inserts a unit distance δ, in practical, the needle will move β which is longer than δ. We assume that, in the insertion distance β, the penetrated material is compressed with ratio r. Then, the unit distance of needle insertion could be achieved by $\beta = \delta/r$.

The compressive ratio r should be varying due to the disparate tissues and needles. Based on research in liver deformation [15], we can acquire the compressive ratio of normal liver tissue which is calculated and experimented through probabilistic and inverse finite element. The results show that, under the stress N_p, the compressed ratio follows a normal distribution with μ_ε and σ_ε. For the purpose of robust planning which provide maximally secure insertion trajectory, we use the highest stress in the experiment N_{pmax} and corresponding compressive ratio $r_{pmin} = \mu_\varepsilon - 3\sigma_\varepsilon$.

Finally, we implement Minkowski sum [36] on the obstacle polygons which can extend the border of segmented obstacles and counteract the influence of tissue deformation. The target region is defined by a circle with center points $\mathbf{t}$ and radius r_{pmin}.

Step two: cost characterization for target patterns

The treatment area always has various shapes and properties [3]. The target such as tumor always has different fractions and stiffness [16]. If the needle cannot penetrate treatment area after several attempts, the postoperative results will be significantly affected. The repetitive insertion will potentially

change the target's location and cause stretch which can lead to unpredictable effect in postoperative recovery.

To achieve a high penetration rate of treatment area in the first attempt, the angle of insertion should be specifically selected based on the patterns of treatment areas. Normally, the stiffness of target is higher than that of the normal tissue. Hence, the vertical insertion with respect to the center of target is always preferred. To incorporate this function to the MDPs path planning method, we modify the cost function to realize the robust purpose in this situation.

We quote the concept of cost in traditional MDPs method but append angle information to represent the complexity of target's patterns. Five costs are assumed independently to represent four types of damage during the needle insertion and rewards. Normally, these costs $C_n = C(p)$ are set as fixed values with respect to the position in the workspace which $p = (p_y, p_x)$. For the purpose of encouraging the needle insertion through specific angles into the target, we introduce the needle direction θ into the cost function. Therefore, the cost function depends on both needle tip position and insertion angle on the target. Following the MDPs path planning framework, the system will generate a control sequence with lowest cost which attains the goal of guiding the needle insertion with specific angle. The new costs are denoted as $C_n = C(p, \theta)$. Allocating the specific number in the cost highly depends on the targets recognized by medical professionals.

Step three: robust MDPs for path planning

Flexible needle does not fully response to its manipulation in reality. The main reason is the uncertainty in needle–tissue interaction which cannot be accurately estimated. In traditional MDPs path planning, the motion uncertainty $P_{ij}(u)$ is defined as a single transition probability of an action from initial state to target state. However, this motion uncertainty is highly variable since the properties of both needles and tissues are different in every single surgery. Furthermore, determining the value of uncertainty parameter for every patients and surgical tools is impractical. Hence, to enhance the robustness and efficiency of path planning, the motion uncertainty should be represented by a certain range instead of one specific number.

Therefore, we need to consider a range of transition probability in MDPs to maximize the performance under the most adversarial distribution of the uncertainty parameters which are the worst cases with highest costs among a set of transition probability. Hence, in flexible needle steering, this issue has become that of generating a robust policy which can achieve minimum expected costs under the worst admissible distribution of uncertain transitions. This issue has been solved by a robust MDPs method [22] which will be introduced later in this section.

The MDPs could be constructed as below: The map is defined as a rectangle with height $y_{\max}$ and depth $x_{\max}$. The obstacles are processed in previous sections. During needle insertion, the state S of needle tip in the soft tissue could be fully characterized by the direction angle θ, the bevel direction b and the needle tip position $p = (p_y, p_x)$. Since a bevel needle is used in the workspace, the bevel direction could be defined by bevel-left ($b = 0$) or bevel-right ($b = 1$). For control actions, there are two actions implemented in this framework: (1) Insert the needle ($u = 1$) into the tissue with a distance δ and (2) perform the rotation ($u = 0$).

The costs are selected in step two. C_i is selected as the cost for needle insertion with a unit distance δ that slightly damage the normal tissue. C_e is chosen to present the cost that needle reaches the border. C_o presents the cost that the needle collides with obstacles. C_r presents the cost of needle rotation. The rewards of reaching the target are represented by C_t.

The workspace is constructed in a grid world with same length and height Δ based on the segmented medical images. Therefore, if we equally subdivide the trajectory circle into N_c and introduce θ to denote the specific direction, the state in path planning framework could be represented by $S = \{q, \theta, b\}$ and the total number of the states in MDPs is

$$N = 2N_cN_s = \frac{4\pi r y_{\max} x_{\max}}{\Delta^2 \delta}.$$

The transition probability is represented by $P_{ij}(u)$, which i denotes current state, and j denotes the nest state. The cost c of a transition is denoted as $c(i, u, j)$ with current state, next state and specific action. So, for a given action sequence $a = [u_0, u_1, \dots]$, the total cost $C(x_0)$ in the initial state x_0 is

$$\begin{aligned} C(x_0) &= E\left[\sum_{k=0}^{\infty} c(x_i, u_k, x_j)\right] \\ &= \sum_{k=0}^{\infty} \sum_{x_{k+1}=1}^{N} P_{ij}(u_k) c(x_i, u_k, x_j). \end{aligned}$$

To minimize the total cost, provide the robust policy and prevent the potential worst case caused by a range of uncertainty $P_{ij}(u)$, we implement the robust MDPs approach in related research [22]. The robust counterpart of the Bellman equation has the form, for all i,

$$\begin{aligned} C^{\star}(i) &= \min_u \max_{P \in \mathcal{P}} E[c(i, u, j) + C^{\star}(j)] \\ &= \min_u \max_{P_{ij} \in \mathcal{P}} \sum_{j=1}^{N} P_{ij}(u)(c(i, u, j) + C^{\star}(j)). \end{aligned}$$

Here $\mathcal{P}$ is the uncertainty set containing feasible transitions P_{ij} following uniform distribution. The above equations are polynomial time solvable if the uncertainty set obeys rectangularity property and is a polytope, ellipsoid or an intersection of ellipsoids and polytopes. The goal of such formulation is to protect the system from the worst-case realizations of uncertain parameters, i.e., transition probabilities. We will design a specific form of $\mathcal{P}$ in our experiments, and we refer interested reader to robust MDPs [22] for more details.

Experiments

To test the robustness of our new algorithm and the feasibility of steering flexible needles on surgical robot, we conducted two experiments. In the first experiment, the robust path planning algorithm was used to manipulate a prototype robot [33,34] to execute RFA needle insertion on a phantom model. The second experiment was a computer simulation that compared the performance of traditional MDPs algorithm and our robust path planning method for RFA simulation using patient CT data.

Figure 2 shows the end effector of a robotic manipulator in our prototype image-guide radio-frequency ablation surgical system which can perform large and multiple liver tumors ablation through single insertion point (SIP) on the patient skin [33,34]. Compared with traditional liver resection surgery, the ablation through SIP can significantly reduce the invasion and enhance the postoperative recovery [33]. The comprehensive setup of this prototype robotic system during an animal experiment is shown in Fig. 3.

There are many steerable needles [37]. We used a flexible RITA RFA needle (RITA®, StarBurst™, USA) shown in Fig. 4 in our experiments. The RITA RFA needle is currently used in our collaborating hospital.

Characterization of tissue–needle interaction

The characterization aims to accurately study the interaction between flexible RITA RFA needle and phantom. The phantom material which we used to approximate the tissue behavior is made by mixing 10 g agarose powder (SeaKem® LE Agarose, USA) with 900 ml water. The characterization results were used in the phantom experiment.

The experimental setup for characterization is shown in Fig. 5. The prototype robot will perform a vertical 10-cm needle insertion in 20 s. The camera will take a picture in every 2 s to record the position of needle tips. Then, the trajectory of needle tip will be re-constructed on each picture. Data analysis is performed by Tkinter, PIL and matplotlib library on Python.

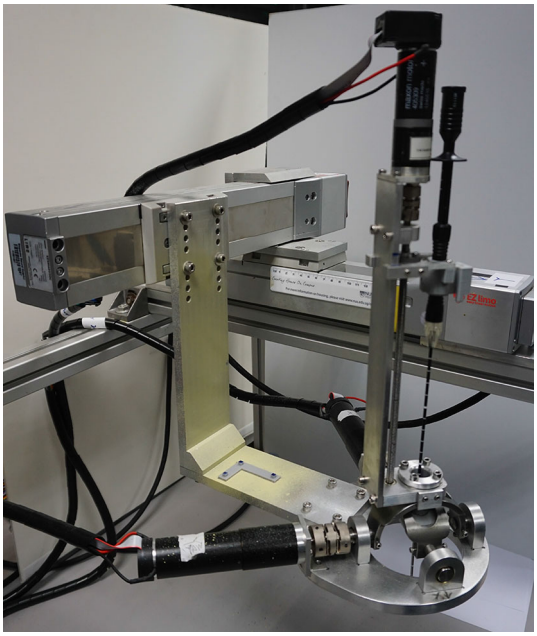

Fig. 2 The needle insertion robot for image-guided radio-frequency ablation surgical system

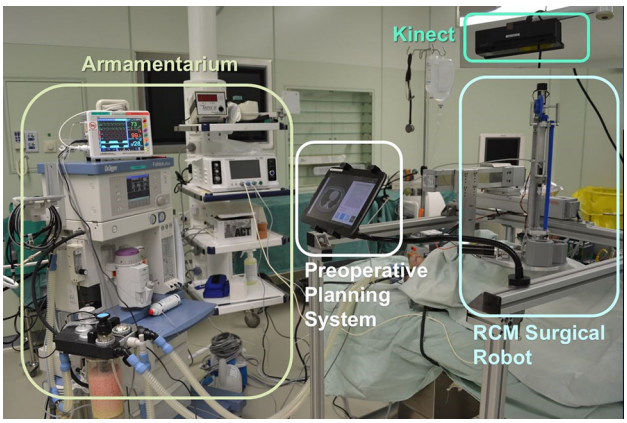

Fig. 3 Setup of the prototype image-guide radio-frequency ablation surgical system

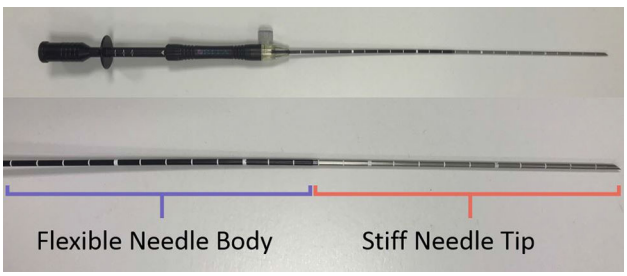

Fig. 4 Flexible RITA RFA needle

The needle tip locations in the phantom are shown in Fig. 6. The positions of needle tips are not identical to the trail of needle body due to deformation. Figure 6c also substanti-

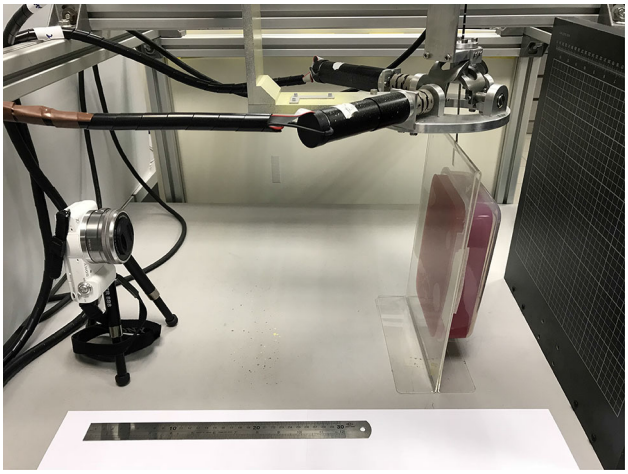

Fig. 5 Experimental setup for characterization

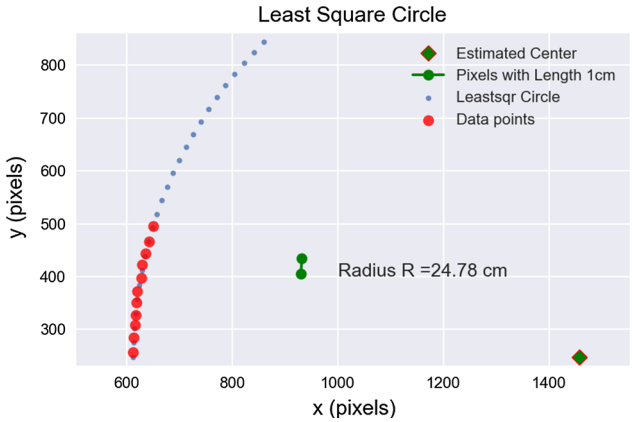

Fig. 7 The optimization result of least square optimizer

ates the uncertainty of needle–tissue interaction which causes different insertion length in disparate time steps.

After obtaining trajectory data, a least square optimizer was used to fit the nonlinear trajectory. Based on the optimization results shown in Fig. 7, the trajectory for flexible needle in phantom is an approximate circular arc with radius $R = 24.78$ cm and error ± 0.25 cm when the insertion depth was less than or equal to 10 cm. The experimental results are also supported by related research [11] which has reported that the trajectory of a flexible needle insertion is an approximate circle with radius R.

Liver tissue is not transparent unlike the phantom material; it is also difficult to shape regularly for testing. The above method could not be repeated to study the flexible needle–liver tissue interaction. Unique measuring apparatus was used to measure the two important parameters (k and l_2) of the unicycle model under fluoroscopy for liver tissue characterization [11]. It has been shown that the bevel-based steering in real tissue follows similar trajectory generated in homogeneous rubber phantom. Similarly, we assume that the needle–liver tissue interaction in liver tissue is an approximate circle as shown in Fig. 6.

Phantom experiment using robust path planning method

Phantom experiment was designed and conducted to validate the feasibility of steering needle using robust path planning method with our prototype surgical robot.

The phantom consisted of simulated soft tissue (10 g SeaKem LE Agarose powder with 900 ml water), obstacles (3D printing components with blue marker) and target (marked on phantom surface with white marker). Firstly, a map with $x_{\max} = 10$ cm and $y_{\max} = 10$ cm was constructed and segmented. The discrimination of the control circle was defined as $N_c = 200$ and $\delta = 2\pi R/N_c$, and R was calculated in the characterization section. The unit distance of the workspace was set as $\Delta = 0.2$ cm. Hence, the total number of the states was $N = 2N_cN_s = 4\pi R y_{\max} x_{\max}/\Delta^2\delta = 1{,}000{,}000$. The cost parameters used in path planning algorithm were $C_i = 1$, $C_r = 10$, $C_o = 1000$, $C_e = 100$ and $C_t = -1000$. The simulation results from insertion points (16, 0) and (25, 0) are shown in Fig. 8.

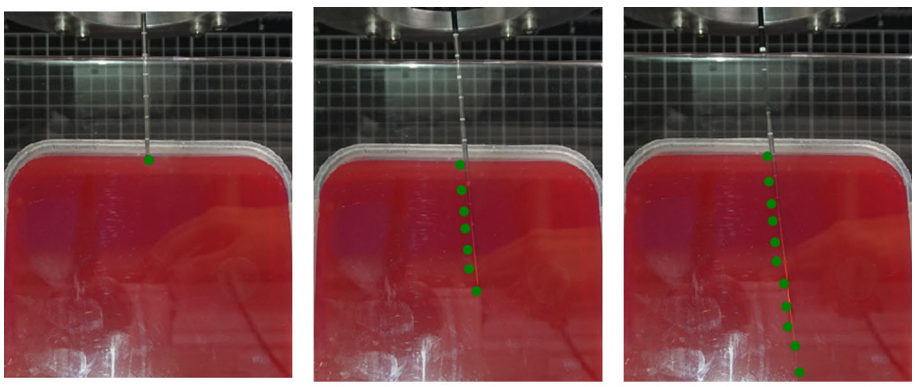

(a) (b) (c)

Fig. 6 The trajectory generated by RITA flexible needle on phantom when time step $t = 0$, $t = 6$ and $t = 10$, respectively. Green dots indicate the location of needle tip for each time step

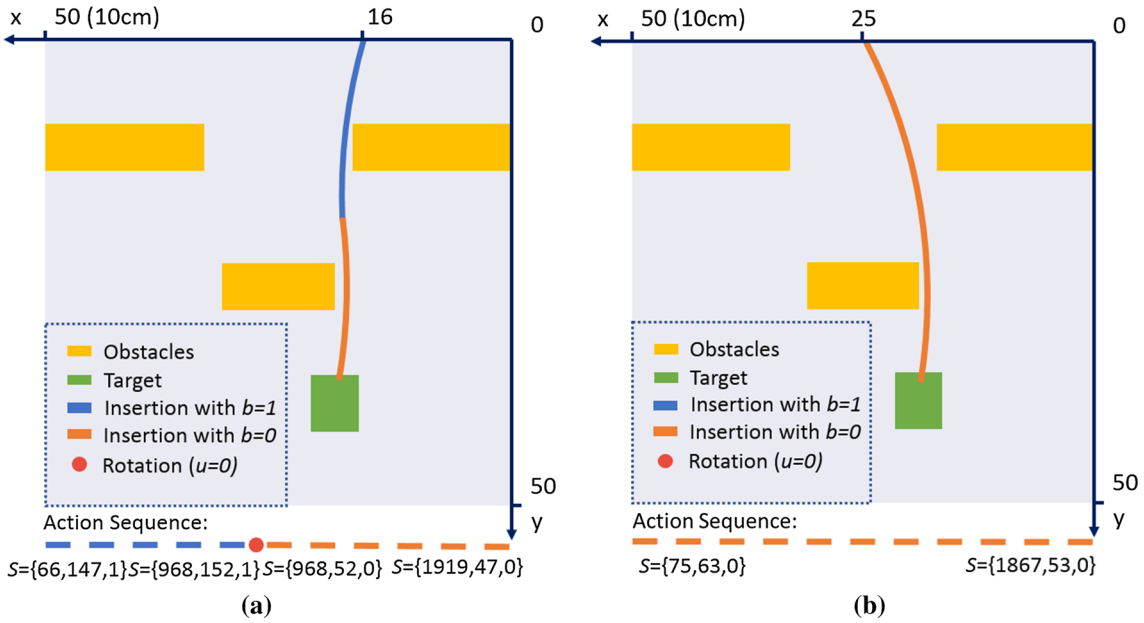

Fig. 8 First plan starts from (16, 0) and takes 12 time steps to complete the task. Five time steps are taken to insert the needle from state $S = \{66, 147, 1\}$ to $S = \{968, 152, 1\}$, 1 time step to rotate and 6 time steps to insert from state $S = \{968, 52, 0\}$ to $S = \{1919, 47, 0\}$. The second plan starts from (25, 0) and takes 11 time steps to navigate from state $S = \{75, 63, 0\}$ to $S = \{1867, 53, 0\}$. **a** Recommended policy and predicted trajectory on insertion point (16, 0). **b** Recommended policy and predicted trajectory on insertion point (25, 0)

The needle was steered by the prototype robotic system from designated location according to the policy derived using the robust path planning algorithm. The phantom experimental results are shown in Fig. 9. The flexible needle had successfully avoided the obstacles and reached the target in all five trails.

RFA simulation using real patient's CT Data

In this computer simulation, the robust path planning method and traditional MDPs algorithm [9,20,21] would generate two independent optimal action sequences to steer the flexible needle toward the suspected liver tumor area using real patient's CT data. All obstacles and target areas had been segmented preoperatively by our collaborate medical professionals.

Two crucial indicators were calculated to represent the robustness and accuracy of different algorithms: total avoidance probability P_a and success rate P_s. Success rate P_s is the rate of successful insertion among 1000 trials by the following different planning algorithms. Probability P_a is the rate of totally avoiding the obstacles and sensitive tissues in 1000 trials.

The path planning software was implemented using MATLAB. The workspace was defined as a rectangle on the CT image with $x_{\max} = 20$ cm and $y_{\max} = 10$ cm. The discrimination of the control circle was defined as $N_c = 100$ and $\delta = 2\pi r/N_c$. The unit distance of the workspace was set as $\Delta = 0.2$ cm. Hence, the total number of the states was $N = 2N_cN_s = 4\pi r y_{\max} x_{\max}/\Delta^2\delta = 1{,}000{,}000$. The cost parameters used in path planning algorithm were $C_i = 1$, $C_r = 10$, $C_o = 1000$, $C_e = 100$ and $C_t = -100$, respectively.

The compressive ratio of the liver tissue was selected as follows: $r_{pmin} = \mu_\varepsilon - 3\sigma_\varepsilon = 0.71 - 3 * 0.2 = 0.65$ and stress $N_{pmax} = 3000\ \mathrm{Nm}^{-2}$ [15]. This covers most of the cases in liver tissue deformation since the real stress will not exceed N_{pmax} in needle insertion. Considering the principle of vertical insertion, we update the cost function of C_t as follows:

$$C_t = \begin{cases} C_t(p,\theta) = 100 & 37 > \theta > 13 \text{ and } 87 > \theta > 63 \\ C_t(p,\theta) = 150 & \text{otherwise.} \end{cases}$$

We assume that the flexible needle will follow a circle trajectory with radius $R = 10$ cm and slide a unit distance δ after reaching the designated position with a probability between 10 and 20%. This assumption follows that of previous works [9,20] which introduce a magnified bevel 0.83 mm diameter solid Nitinol cylinder (21-gauge needle from Nitinol Devices and Components™, USA). This superelastic material is an alloy of approximately 55% nickel and 45% titanium, which can satisfy many clinical inference in liver thermal ablation and intracranial hemorrhage (ICH) [11,12].

The uncertainty set, $\mathcal{P} = \{P_{ij} | 0.1 \le P_{ij} \le 0.2, \sum_j P_{ij} = 1\}$. The insertion procedure could be stuck unpredictably

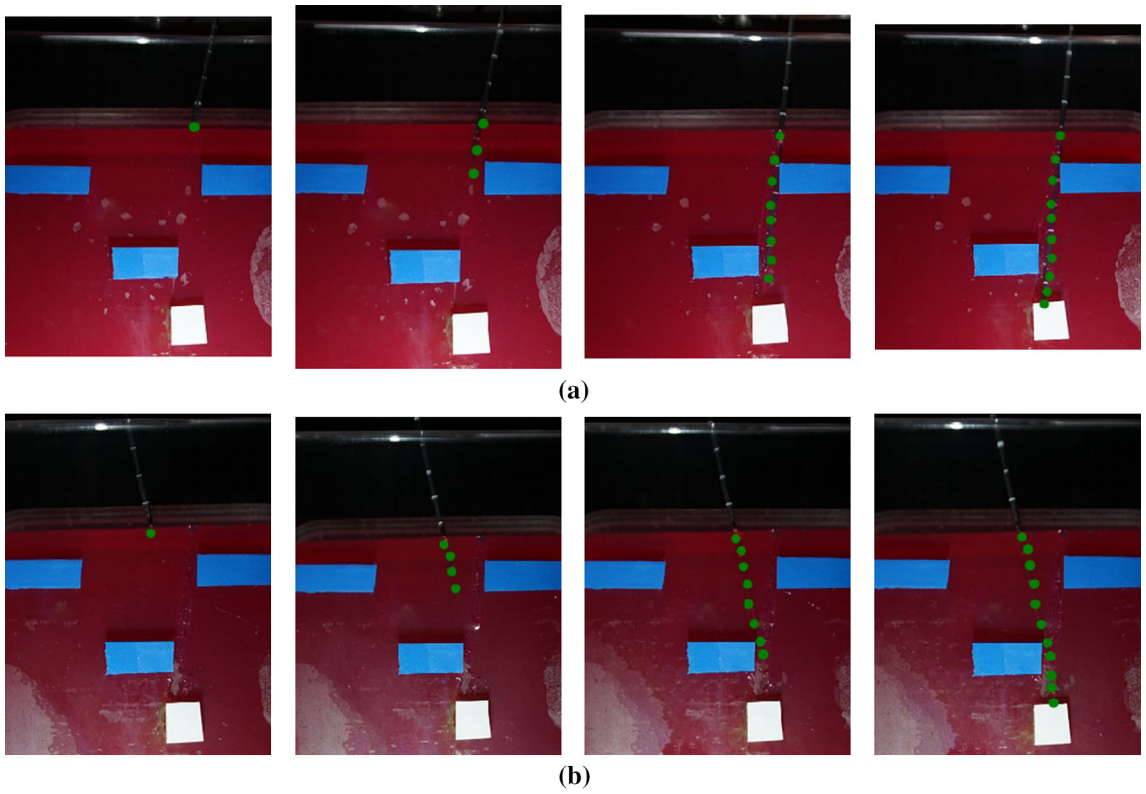

Fig. 9 Surgical robot implements the policy shown in Fig. 8 and performs the needle insertion at point (16,0) and (25,0). Green dots indicate the location of needle tip for each time step. **a** One robotic insertion trial following the policy at point (16,0). **b** One robotic insertion trial following the policy at point (25,0)

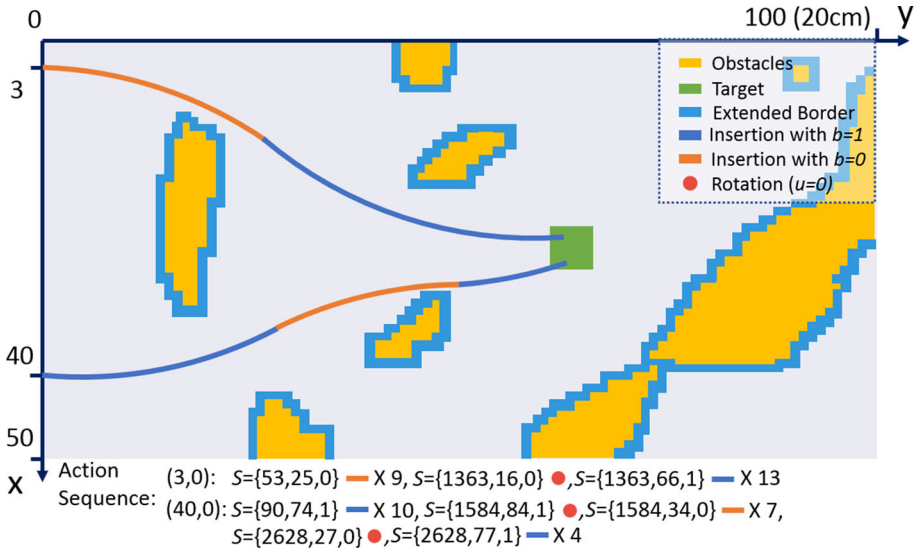

Fig. 10 This figure shows the predicted trajectory and optimal policy generated by robust path planning method at points (3, 0) and (40, 0). At point (3, 0), optimal policy recommends to take 23 time steps with only one rotation action to reach the target. At point (40, 0), optimal policy recommends to take 23 time steps with two rotation actions to reach the target

with a probability between 0% and 5%. The uncertainty set, $\mathcal{P} = \{P_{ij} | 0 \leq P_{ij} \leq 0.05, \sum_j P_{ij} = 1\}$.

For comparison, another experiment is conducted using traditional MDPs path planning method with 15% probability of slides and 5% probability of movement failure. In practice, parameters should be chosen according to different surgical areas on the patients bodies, various patient conditions and surgical instruments. These medical data could be organized and automatically selected in cognitive engine [38,39]. The predicted trajectories and policies for two insertion points are shown in Figs. 10 and 11, respectively.

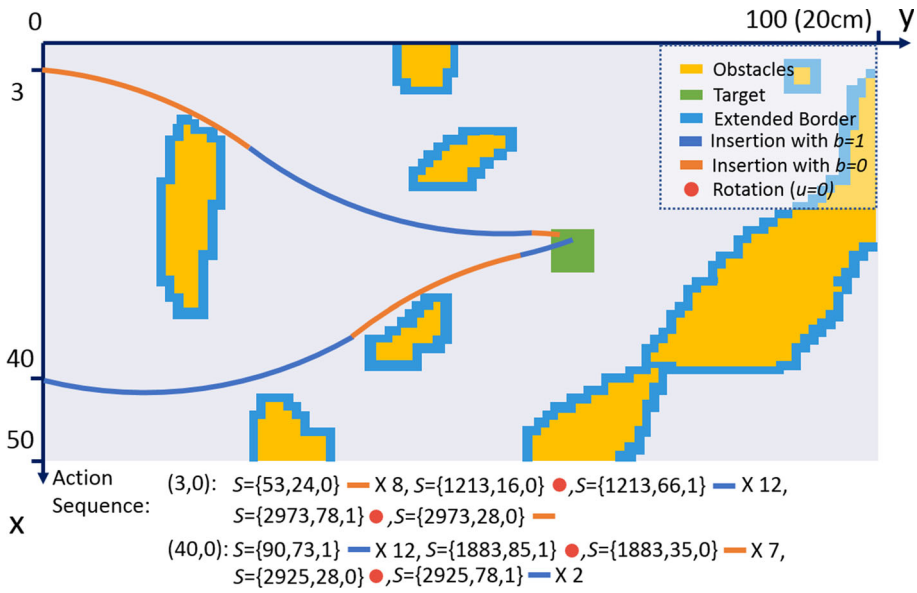

Fig. 11 This figure shows the predicted trajectory and optimal policy generated by traditional MDPs algorithm at points (3, 0) and (40, 0). At point (3, 0), optimal policy recommends to take 23 time steps with two rotation actions to reach the target. At point (40, 0), optimal policy recommends to take 23 time steps with also two rotation actions to reach the target

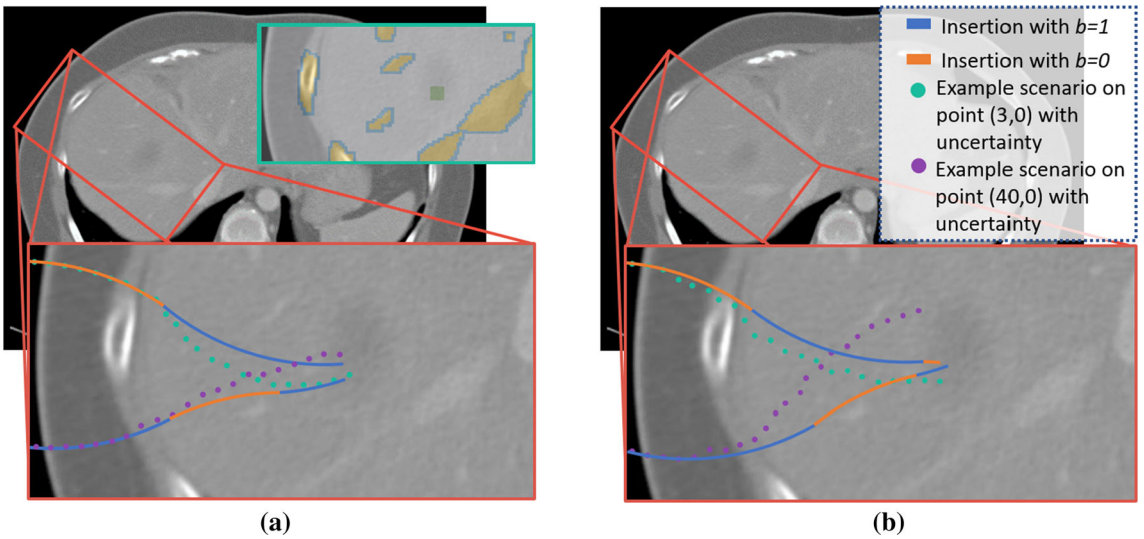

Fig. 12 The predicted trajectories for each algorithm on CT images at two insertion points. **a** Robust path planning method. **b** Traditional path planning with single transition probability

Since the control circle was defined on the grid workspace, the error between estimated trajectory point p and real point p_r was $e = \Delta\sqrt{2}/2$. The rotation action $u = 0$ would cause an error $e = \Delta\sqrt{2}$ because of changing position of control center. Hence, the final error at the end point of trajectory was bound by $E = \Delta\sqrt{2}(n + 0.5)$ where n is the number of rotation action $u = 0$ in policy.

We demonstrated the policy on two designated insertion points. The trajectories of each algorithm are also shown on the CT image in Fig. 12. Each algorithm generated one example scenario on two designated insertion points impacted with uncertain needle–tissue interaction (a range of uncertain transition probability). It is critical to note that the trajectories under uncertain circumstance could be bounded by the robust path planning policy which maximize the probability in avoiding obstacles (vessels and bones). In contrast, two scenarios in Fig. 12b show that the policy generated by traditional MDPs algorithm cannot overcome uncertain circumstance which causes deviation in steering.

The statistical results for two scenarios are shown in Table 1. The result is significant at the area ahead of insertion point (3, 0) which is a narrow workspace with large obstacles. The robust path planning method achieves a slightly higher success rate ($P_s = 68.2\%$) but a huge improvement in total avoidance probability ($P_a = 92.4\%$) which is $P_a = 47.3\%$ in comparison. This result proves that the policy generated by robust path planning method can prevent the worst cases (e.g., damaging the obstacles) especially in complex opera-

Table 1 The simulation results for traditional MDPs method and robust path planning algorithm on two example points. P_s and P_a are calculated among 1000 trails, respectively, in simulation

Methods	Insertion point	Success rate P_s (%)	Total avoidance probability P_a (%)	Error (mm)
Traditional MDPs	(40,0)	73.5	87.2	± 4
	(3,0)	66.9	47.3	± 4
Robust planning	(40,0)	80.8	94.8	± 4
	(3,0)	68.2	92.4	± 2

Table 2 The simulation results for traditional MDPs method and robust path planning algorithm. P_s and P_a are calculated among 1000 trails, respectively, in simulation

Insertion point	P_a for robust planning (P_{ar}) (%)	P_s for robust planning (P_{sr}) (%)	P_a for traditional MDPs (P_{at}) (%)	P_s for traditional MDPs (P_{st}) (%)	State index
(2,0)	79.2	70.1	75.5	67.5	0
(3,0)	92.4	68.2	47.3	66.9	1
(4,0)	83.4	63.0	80.9	57.3	2
(5,0)	90.3	45.5	62.4	54.9	3
(6,0)	94.4	71.7	69.6	75.5	4
(7,0)	89.2	57.4	59.2	62.8	5
(8,0)	88.3	37.5	3.7	48.2	6
(9,0)	87.1	41.7	0	47.5	7
(10,0)	38.6	70.8	40.5	70.9	8
(11,0)	64.0	64.6	0	52.0	9
(12,0)	51.4	71.3	0	45.9	10
(27,0)	63.2	51.9	0	64.6	11
(28,0)	68.0	82.3	0	68.8	12
(29,0)	83.8	65.8	0	72.5	13
(30,0)	64.0	75.0	0	64.9	14
(31,0)	93.9	77.7	0	72.8	15
(32,0)	80.9	63.7	58.3	72.5	16
(33,0)	78.9	75.9	75.5	66.7	17
(34,0)	91.1	75.9	87.6	71.6	18
(35,0)	94.7	74.4	83.8	72.2	19
(36,0)	94.8	76.2	94.6	73.2	20
(37,0)	88.8	77.2	88.0	74.9	21
(38,0)	91.6	80.7	89.7	77.4	22
(39,0)	94.0	79.7	92.4	77.9	23
(40,0)	94.8	80.8	87.2	73.5	24
(41,0)	88.3	75.8	91.2	76.1	25
(42,0)	90.6	74.2	7.4	21.6	26
(43,0)	95.6	75.0	13.5	25.7	27
(44,0)	87.6	73.8	12.8	31.5	28
(45,0)	93.8	76.6	15.0	24.5	29
(46,0)	95.9	71.6	10.7	37.6	30
(47,0)	96.0	64.1	11.2	26.5	31
(48,0)	90.7	74.0	16.7	28.4	32
(49,0)	91.7	75.7	25.5	39.6	33

Table 3 Three groups of T test results. Each group contains two results for P_a and P_s, respectively

Conditions (with alpha level $a = 0.05$)	Groups	t value	p value	Results
All available points	P_a	7.133	$p < 0.0005$	$p < a$
	P_s	3.421	$0.001 > p > 0.0005$	$p < a$
Condition 1	P_a	4.256	$p < 0.0005$	$p < a$
	P_s	3.725	$0.001 > p > 0.0005$	$p < a$
Condition 2	P_a	1.904	$0.05 > p > 0.025$	$p < a$
	P_s	3.849	$0.005 > p > 0.001$	$p < a$

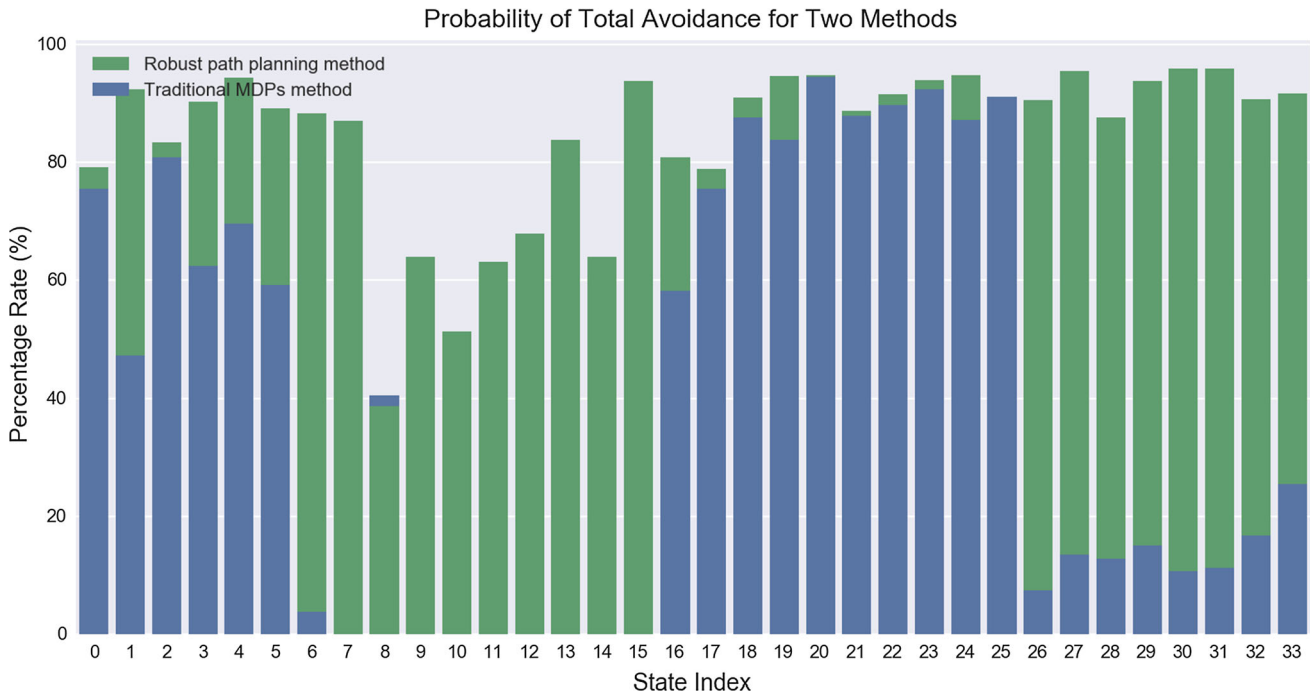

Fig. 13 Probability of total avoidance P_a for two methods

tive circumstance with a range of uncertain transition. This operative environment is more realistic in practical application than assuming one transition uncertainty in traditional MDPs.

Compared with operation region at point $(3, 0)$, the area associated with $(40, 0)$ is wider with less obstacles. Robust path planning method achieves $P_s = 80.8\%$ and $P_a = 94.8\%$ which are also higher than that of the traditional MDPs method in 1000 trials.

The experimental result for all available insertion points is shown in Table 2. From these points, flexible RFA needles are physically possible to be steered toward target area. To distinctly evaluate the performance of the two algorithms, success rate P_s and total avoidance probability P_a for each available points are plotted in Figs. 13 and 14, respectively.

Six groups of statistical analysis (T test) were performed to show the significance of robust path planning algorithm. First two analyses were based on the overall performance at all available insertion points. Third and fourth analyses are performed at points which can perform an acceptable needle insertion steered by both algorithms. These points satisfy Condition 1.

Condition 1 $\{P_{ar} > 80.0\% \textit{ and } P_{sr} > 70.0\%\}$ *or* $\{P_{at} > 80.0\% \textit{ and } P_{st} > 70.0\%\}$

The last two analyses were performed at the points which had already achieved high P_a and P_s in traditional MDPs method. These groups demonstrate the significance of our robust path planning method on points that traditional MDPs method has already achieved superior results. These points satisfy Condition 2.

Condition 2 $\{P_{ar} > 80.0\% \textit{ and } P_{sr} > 70.0\%\}$ *and* $\{P_{at} > 80.0\% \textit{ and } P_{st} > 70.0\%\}$

Based on the statistical analysis shown in Table 3, the p value p is smaller than the default alpha value a for P_a and P_s in each condition. Therefore, the null hypothesis could be rejected and the significance could be demonstrated by the

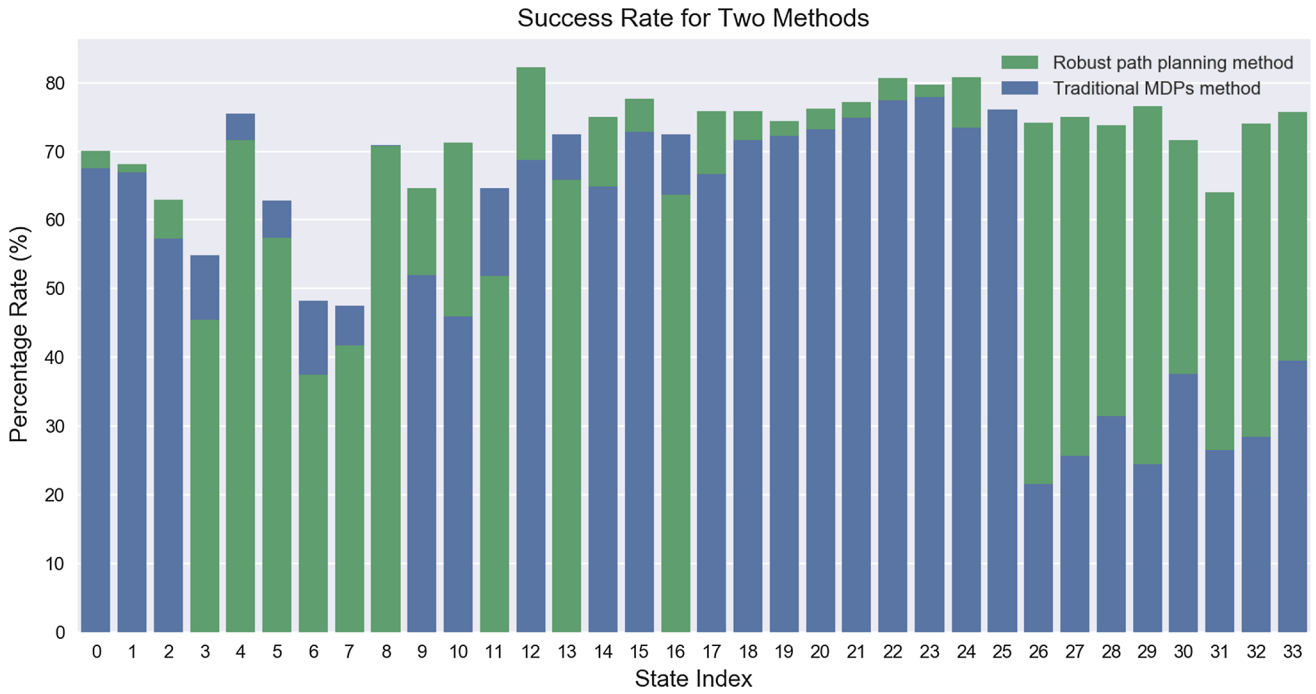

Fig. 14 Success rate P_s for two methods

range of the p value shown in Table 3. Our result indicates that the robust path planning method can achieve higher robustness and success rate than that of traditional MDPs method at the same insertion points. It also increases the overall robustness and success rate.

Conclusion

In this paper, a new robust path planning method is developed to steer flexible needle in soft tissue. This method uses preoperative medical images to construct the work space and implements MDPs and DP to generate an optimal control sequence for needle insertion. Compared with previous work [9,20,21], our algorithm achieves high accuracy and high avoidance probability (shown in Tables 1 and 2, respectively) in computer simulation using patient's CT data. The statistical analysis shown in Table 3 demonstrates a significance improvement in robustness and accuracy. The phantom experimental results show the feasibility of our algorithm in steering common flexible needle using a robot.

Hence, based on our experiments and computer simulation, our algorithm can achieve a more secure and robust result. This result is based on the following assumptions: non-negligible soft tissue deformation behavior, highly varying patterns of treatment areas and unpredictable motion uncertainty of needle–tissue interaction during complex operation. However, in vivo experiment with real tissue is necessary to further validate the clinical viability of our method.

We were aware that our current research may have limitation in predicting the needle–tissue interaction under the influence of multi-layer tissues. It is difficult to collect data during real operation. For future works, we would design customized apparatus to measure the needle–tissue interaction (transition uncertainty and characterization) during animal experiment. More patients' CT data will be acquired to fully test the robust path planning method. Multiple reinforcement learning methods will be used to improve the robust path planning method for processing large state space in 3D medical imaging workspace and to consider the effect of multi-layer tissue. The physical properties of various existing flexible needles will be measured and modeled to enhance the accuracy of planning.

Funding The research and development of the prototype image-guide radio-frequency ablation surgical system was supported in parts by research grants from Singapore Agency of Science and Technology (A*Star) and Ministry of Education, Singapore, respectively.

Compliance with ethical standards

Conflict of interest The authors declare that they have no conflict of interest.

Human participants All procedures performed in studies involving human participants were in accordance with the ethical standards of the institutional and/or national research committee and with the 1964 Helsinki Declaration and its later amendments or comparable ethical standards.

Informed consent Informed consent was obtained from all individual participants included in the study.

References

1. Fuchs KH (2002) Minimally invasive surgery. Endoscopy 34(02):154–159
2. Rosen M, Ponsky J (2001) Minimally invasive surgery. Endoscopy 33(04):358–366
3. Abolhassani N, Patel R, Moallem M (2007) Needle insertion into soft tissue: a survey. Med Eng Phys 29(4):413–431
4. Doi K (2007) Computer-aided diagnosis in medical imaging: historical review, current status and future potential. Comput Med Imaging Graph 31(4):198–211
5. Nath S, Chen Z, Yue N, Trumpore S, Peschel R (2000) Dosimetric effects of needle divergence in prostate seed implant using 125i and 103pd radioactive seeds. Med Phys 27(5):1058–1066
6. Carr JJ, Hemler PF, Halford PW, Freimanis RI, Choplin RH, Chen MYM (2001) Stereotactic localization of breast lesions: how it works and methods to improve accuracy. Radiographics 21(2):463–473
7. Taschereau R, Pouliot J, Roy J, Tremblay D (2000) Seed misplacement and stabilizing needles in transperineal permanent prostate implants. Radiother Oncol 55(1):59–63
8. Narayana V, Roberson PL, Winfield RJ, Kessler ML, McLaughlin PW (1996) Optimal placement of radioisotopes for permanent prostate implants. Radiology 199(2):457–460
9. Alterovitz R, Branicky M, Goldberg K (2008) Motion planning under uncertainty for image-guided medical needle steering. Int J Robot Res 27(11–12):1361–1374
10. Donaldson MS, Corrigan JM, Kohn LT (2000) To err is human: building a safer health system, vol 6. National Academies Press, Washington
11. Robert J, Webster III, Kim JS, Cowan NJ, Chirikjian GS, Okamura AM (2006) Nonholonomic modeling of needle steering. Int J Robot Res 25(5–6):509–525
12. Webster RJ, Memisevic J, Okamura AM (2005) Design considerations for robotic needle steering. In: Proceedings of the 2005 IEEE international conference on robotics and automation, ICRA 2005. IEEE, pp 3588–3594
13. Leong F, Huang W-H, Chui C-K (2013) Modeling and analysis of coagulated liver tissue and its interaction with a scalpel blade. Med Biol Eng Comput 51(6):687–695
14. Fu YB, Chui CK (2014) Modelling and simulation of porcine liver tissue indentation using finite element method and uniaxial stress–strain data. J Biomech 47(10):2430–2435
15. Fu YB, Chui CK, Teo CL (2013) Liver tissue characterization from uniaxial stress-strain data using probabilistic and inverse finite element methods. J Mech Behav Biomed Mater 20:105–112
16. O'Reilly MS, Boehm T, Shing Y, Fukai N, Vasios G, Lane WS, Flynn E, Birkhead JR, Olsen BR, Folkman J (1997) Endostatin: an endogenous inhibitor of angiogenesis and tumor growth. Cell 88(2):277–285
17. Abayazid M, Vrooijink GJV, Patil S, Alterovitz R, Misra S (2014) Experimental evaluation of ultrasound-guided 3d needle steering in biological tissue. Int J Comput Assist Radiol Surg 9(6):931–939
18. Vrooijink JG, Abayazid M, Patil S, Alterovitz R, Misra S (2014) Needle path planning and steering in a three-dimensional non-static environment using two-dimensional ultrasound images. Int J Robot Res 33(10):1361–1374
19. Patil S, Burgner J, Webster RJ, Alterovitz R (2014) Needle steering in 3-d via rapid replanning. IEEE Trans Robot 30(4):853–864
20. Alterovitz R, Lim A, Goldberg K, Chirikjian GS, Okamura AM (2005) Steering flexible needles under Markov motion uncertainty. In: 2005 IEEE/RSJ international conference on intelligent robots and systems, (IROS 2005). IEEE, pp 1570–1575
21. Alterovitz R, Siméon T, Goldberg KY (2007) The stochastic motion roadmap: a sampling framework for planning with Markov motion uncertainty. In: Robotics: science and systems, vol 3, pp 233–241
22. Pengqian Y, Huan X (2016) Distributionally robust counterpart in Markov decision processes. IEEE Trans Autom Control 61(9):2538–2543
23. DiMaio S, Salcudean SE (2003) Needle insertion modeling and simulation. IEEE Trans Robot Autom 19(5):864–875
24. DiMaio PS, Salcudean SE (2005) Needle steering and motion planning in soft tissues. IEEE Trans Biomed Eng 52(6):965–974
25. Glozman D, Shoham M (2006) Flexible needle steering for percutaneous therapies. Computer Aided Surg 11(4):194–201
26. Kallem V, Cowan NJ (2009) Image guidance of flexible tip-steerable needles. IEEE Trans Robot 25(1):191–196
27. Shahriari N, Roesthuis RJ, van de Berg NJ, van den Dobbelsteen JJ, Misra S (2016) Steering an actuated-tip needle in biological tissue: fusing fbg-sensor data and ultrasound images. In: 2016 IEEE international conference on robotics and automation (ICRA). IEEE, pp 4443–4449
28. Suetens P (2017) Fundamentals of medical imaging. Cambridge University Press, Cambridge
29. Thie PR (1983) Markov decision processes. Comap, Incorporated, Bedford
30. Bertsekas DP, Bertsekas DP, Bertsekas DP, Bertsekas DP (1995) Dynamic programming and optimal control, vol 1. Athena Scientific, Belmont
31. Mostafa A, Fouad A, Elfattah MA, Hassanien AE, Hefny H, Zhu SY, Schaefer G (2015) Ct liver segmentation using artificial bee colony optimisation. Proc Comput Sci 60:1622–1630
32. Norajitra T, Meinzer H-P, Maier-Hein KH (2015) 3d statistical shape models incorporating 3d random forest regression voting for robust ct liver segmentation. In: Proceedings of SPIE, vol 9414, p 941406
33. Duan B, Wen R, Chng C-B, Wang W, Liu P, Qin J, Peneyra JL, Chang Stephen K-Y, Heng P-A, Chui C-K (2015) Image-guided robotic system for radiofrequency ablation of large liver tumor with single incision. In: 2015 12th international conference on ubiquitous robots and ambient intelligence (URAI). IEEE, pp 284–289
34. Yang L, Wen R, Qin J, Chui C-K, Lim K-B, Chang SK-Y (2010) A robotic system for overlapping radiofrequency ablation in large tumor treatment. IEEE/ASME Trans Mechatron 15(6):887–897
35. Liu Y, Kerdok AE, Howe RD (2004) A nonlinear finite element model of soft tissue indentation. Lect Notes Comput Sci 3078:67–76
36. Varadhan G, Manocha D (2006) Accurate Minkowski sum approximation of polyhedral models. Graph Models 68(4):343–355
37. van de Berg NJ, van Gerwen DJ, Dankelman J, van den Dobbelsteen JJ (2015) Design choices in needle steeringa review. IEEE/ASME Trans Mechatron 20(5):2172–2183
38. Tan X, Chng C-B, Duan B, Ho Y, Wen R, Chen X, Lim K-B, Chui C-K (2016) Design and implementation of a patient-specific cognitive engine for robotic needle insertion. In: 2016 IEEE international conference on systems, man, and cybernetics (SMC). IEEE, pp 000560–000565
39. Tan X, Chng C-B, Duan B, Ho Y, Wen R, Chen X, Lim K-B, Chui C-K (2017) Cognitive engine for robot-assisted radio-frequency ablation system. Acta Polytech Hung 14(1):129–145